BIOCHEMISTRY
including biophysical chemistry & molecular biology
Article

Biochemistry **2009,** *48,* 12159–12168 12159
DOI: 10.1021/bi901188s

The MDM2-Binding Region in the Transactivation Domain of p53 Also Acts as a Bcl-X_L-Binding Motif[†]

Huibin Xu,[‡,||] Hong Ye,[‡,||] Nur Eliza Osman,[‡] Kristen Sadler,[‡] Eun-Young Won,[§] Seung-Wook Chi,[§] and Ho Sup Yoon*[,‡]

[‡]*School of Biological Sciences, Nanyang Technological University, 60 Nanyang Drive, Singapore 637551 and* [§]*Medical Proteomics Research Center, KRIBB, 111 Gwahangno, Yuseong-gu, Daejeon 305-806, Korea.* [||]*These authors equally contributed to this work.*

Received July 12, 2009; Revised Manuscript Received November 14, 2009

ABSTRACT: While the transcription-dependent mechanism of p53 has been extensively studied, recently the transcription-independent apoptotic activity of p53 has also been described. Bcl-2 and Bcl-X_L interact with p53 and induce apoptosis. Initially, the p53 DNA-binding domain (p53DBD) was found to bind to Bcl-2 and Bcl-X_L. Later, the p53 N-terminal domain (p53NTD) was reported to be sufficient for inducing the transcription-independent apoptotic activity of p53 and also shown to interact with Bcl-X_L. Here, we further document that the transactivation domain of p53 (p53TAD) in p53NTD alone binds to Bcl-X_L. We demonstrated that the MDM2-binding region (residues S15 to N29, herein referred to as SN15) in p53TAD is the binding site for Bcl-X_L. The binding interface on Bcl-X_L was identified at the hydrophobic pocket formed by the BH1, BH2, and BH3 domains, which also binds to the Bak/Bad BH3 peptides, suggesting Bcl-X_L and MDM2 share a common binding motif in p53TAD. Our NMR structural studies have shown that the SN15 peptide undergoes a conformational change upon binding to Bcl-X_L. A Bcl-X_L/SN15 complex structural model suggests that the SN15 peptide adopts an extended α-helical structure to bind to the hydrophobic pocket on the Bcl-X_L, which is similar to the mode of binding between BH3 peptides and Bcl-X_L.

p53 is a key tumor suppressor protein in the network of the cellular stress response pathway (*1*). It is found to be mutated or lost in more than 50% of all human cancers, which indicates its critical functions in controlling tumor formation (*2*). As a transcription activator, the transcription-dependent apoptosis activity of p53 has been intensively discussed and is accepted as its major tumor suppressor function (*3*). However, several studies have recently found evidence of the transcription-independent apoptotic activity of p53 where p53 mutants with no transcription activity are still able to induce apoptosis (*4*, *5*) and the absence of transcription does not abrogate p53-dependent apoptosis (*6*−*8*). It has also been reported that p53 can trigger cytochrome *c* release from mitochondria in cell-free cytoplasts (*9*).

Based on recent studies, it is believed that a fraction of p53 is localized in the outer membrane of mitochondria to execute transcription-independent apoptosis after activation by death signals (*10*, *11*). Detailed information on the mitochondrial p53 apoptotic mechanism is still accumulating (*12*−*16*). The Bcl-2 family proteins are the key regulators of apoptosis, controlling the permeability of the outer mitochondrial membrane and the release of such death factors as cytochrome *c* (*12*−*14*). Green et al. also demonstrated that PUMA, a proapoptotic BH3-only protein, can release p53 from the p53/Bcl-X_L complex to bind and activate Bax or Bak, thus allowing Bax and Bak to induce mitochondrial permeabilization (*15*). Another proapoptotic protein Bad was shown to be upregulated by p53 and forms a complex with p53 at the mitochondria and induces apoptosis (*16*). This model explains the function of cytoplasmic p53, integrates the functions of p53 with the Bcl-2 family proteins, and supports the hypothesis that the complex formation of p53 and Bcl-X_L is of importance in p53 transcription-independent apoptotic activity.

A recent study on p53/Bcl-X_L revealed that Bcl-X_L binds to p53 on its DNA-binding domain (*12*, *17*). Interestingly, on the other hand, the N-terminal domain of p53 (p53NTD) was also shown to be sufficient to induce transcription-independent apoptosis (*18*), and the molecular interaction between Bcl-X_L and p53NTD has also been observed (*19*). Together, these results suggest that, in addition to its DNA-binding domain, p53NTD perhaps plays a particular role in the molecular interaction with Bcl-X_L and the transcription-independent apoptosis pathway of p53.

The p53NTD consists of a transactivation domain (p53TAD) and a proline-rich domain. In the study reported herein, we demonstrated that the MDM2 binding region in p53TAD (residues S15 to N29; hereafter referred to as SN15) is responsible for Bcl-X_L binding. The binding site on Bcl-X_L is located at the hydrophobic pocket formed by the BH1, BH2, and BH3 domains, which also binds to the Bak/Bad BH3 peptides. We present that the SN15 peptide upon forming a complex with Bcl-X_L undergoes a conformational change and adopts a more stable structure with an extended α-helix.

EXPERIMENTAL PROCEDURES

Materials. Rabbit anti-Bcl-X_L antibody (S18) was purchased from Santa Cruz Biotech (Santa Cruz, CA). Goat anti-rabbit IgG was purchased from Kirkegaard and Perry Laboratories (Gaithersburg, MD) and Ni^{2+}-NTA resin from Qiagen (Hilden,

[†]This work was supported by Ministry of Education Singapore ARC Grant ARC 4/04 and in part by a grant from the National R&D Program for Cancer Control, Ministry for Health, Welfare, and Family Affairs, Republic of Korea (0720130).

*To whom correspondence should be addressed. E-mail: hsyoon@ntu.edu.sg. Tel: +65 63162846. Fax: +65 67913856.

Published on Web 11/16/2009

Germany). The GST[1] purification module was purchased from GE Healthcare (Piscataway, NJ) and isopropyl β-D-thiogalactopyranoside (IPTG) from Promega (Madison, WI). [^{15}N]NH_4Cl and [^{13}C]glucose were bought from Cambridge Isotope Laboratories, Inc. (Andover, MA), and all other chemicals were obtained from Sigma-Aldrich (St. Louis, MO).

Protein Expression and Purification. Bcl-X_LΔTMΔloop, in which the C-terminal transmembrane domain and the loop region from M45 to A84 were deleted, and the p53NTD (residues 1−102) proteins were expressed and purified as previously described (*19*, *20*). In this study, Bcl-X_LΔTMΔloop was used for most of the biochemical and structural studies, except one NMR experiment to compare the role of the flexible loop in binding to the SN15 peptide. Thus, Bcl-X_LΔTMΔloop was referred to as Bcl-X_L through the report, unless otherwise specified. The DNA fragment of Bcl-X_LΔTM containing the loop region was cloned into pET29b plasmid to generate the pET29b-Bcl-X_LΔTM plasmid, and the ^{15}N-labeled protein was expressed and purified in a similar way as the Bcl-X_LΔTMΔloop. The DNA fragment coding for p53TAD (residues 1−73) was amplified by polymerase chain reaction and subcloned into the *Nde*I and *Xho*I restriction enzyme sites of the pET16b (Novagen, WI) to generate hexahistidine-tagged p53TAD. The DNA fragments encoding p53NTD and p53TAD were also subcloned into the pGEX4T-1 vector to generate GST-p53NTD and GST-p53TAD, respectively. Proteins were expressed in *Escherichia coli* BL21(DE3) cells in an LB or M9 minimal medium supplemented with [^{15}N]NH_4Cl and/or [^{13}C]glucose. Proteins were first purified on a Ni^{2+}-NTA agarose affinity column (for His-tagged proteins) or a glutathione Sepharose 4B affinity column (for GST fusion proteins). One unit of thrombin per milligram of protein was added and incubated overnight at 4 °C and further purified on a Superdex 75 gel filtration column (GE Healthcare, NJ) preequilibrated with gel filtration buffer (50 mM Tris-HCl, pH 8.0, 50 mM NaCl).

GST Pull-Down Assay. GST or GST fusion proteins (20 μg) were mixed with 20 μg of ligand protein and incubated for 2 h on ice. The protein mixtures were then immobilized on 20 μL of GST beads, washed with PBS beforehand, at 4 °C for 2 h. The samples were gently agitated to avoid precipitation of the GST beads. Following incubation the beads were washed five times with a washing buffer (50 mM HEPES, pH 7.5, 170 mM KCl, 7.5 mM $MgCl_2$, 0.1 mM EDTA, 1 mM DTT, 1% Triton X-100, 10% glycerol, 1% BSA), and proteins were eluted with GST elution buffer (50 mM Tris-HCl, 10 mM glutathione, pH 8.0). The eluted samples were separated on a 12.5% SDS−PAGE followed by Western blot.

Western Blotting. Proteins were separated on 12% SDS−PAGE and transferred to a polyvinylidene difluoride (PVDF) membrane. The membranes were blocked with 5% dry milk in TBS-T buffer (20 mM Tris-HCl, pH 7.5, 140 mM NaCl, 0.05% Tween-20) and subsequently incubated with primary antibody followed by a goat anti-rabbit or goat anti-mouse IgG conjugated to horseradish peroxidase, and the immunoreactive bands were visualized using the Immune-Star Chemiluminescent protein detection system (Bio-Rad Laboratories, Hercules, CA).

[1]Abbreviations: PDB, Protein Data Bank; NMR, nuclear magnetic resonance; NOE, nuclear Overhauser effect; HPLC, high-performance liquid chromatography; FPLC, fast performance liquid chromatography; DTT, dithiothreitol; PBS, phosphate-buffered saline; GST, glutathione *S*-transferase.

Peptide Synthesis. The wild-type p53TAD peptide SN15 (S15 to N29) and phosphorylated SN15 peptide were synthesized by GL Biochem (Shanghai, China). All alanine mutants of the SN15 peptides were synthesized on a Multipep peptide synthesizer (Intavis, Cologne, Germany) using Fmoc chemistry. Amino acids were supplied by Novabiochem, and all other synthesis reagents were from Merck. All reagents were of analytical grade or above. Peptides were cleaved from resin using 95:2.5:2.5 trifluoroacetic acid:triisopropylsilane:water for 4 h, separated from the resin by filtration, and then precipitated in diethyl ether before lyophilization. The crude peptides were purified by preparative reverse-phase HPLC on a Waters 600 system using a C18 Vydac column. Products were confirmed by time-of-flight mass spectrometry (TOF-MS) using an Applied Biosystems 4800 TOF/TOF instrument. Measurements were taken in the reflectron mode with α-cyano-4-hydroxycinnamic acid as the matrix. Product purity (> 95%) was confirmed using an analytical RP-HPLC with a C18 Vydac column installed in a Shimadzu LC system (Shimadzu, Singapore).

Surface Plasma Resonance Experiments. Surface plasma resonance experiments were performed in a HBS buffer (10 mM HEPES, pH 7.4, 150 mM NaCl, 1 mM EDTA, 0.001% Tween-20) with a flow rate of 20 μL/min at 25 °C on a BIAcore 3000 instrument (BIAcore AB, Uppsala, Sweden). Bcl-X_L was immobilized to a channel of the CM5 sensor chip using an amine coupling kit (BIAcore AB), and the control flow-subtracted sensorgrams were obtained. The peptide concentrations ranging from 0.625 to 10 μM for both wild-type SN15 and phosphorylated SN15 peptides. After dissociation, the chip was regenerated using 1 M NaCl and 1 mM NaOH. By monitoring the RU level, we confirmed that the bound analytes were completely washed off before the next injection. Kinetic measurements were carried out, and equilibrium dissociation constants were calculated using BIAevaluation version 3.0 software (BIAcore AB). For each set of curves, integration was performed by fitting the raw binding data to the 1:1 Langmuir binding model. Association (K_{on}) and dissociation (K_{off}) rate constants were calculated directly from the integration. The apparent dissociation equilibrium constant (K_d) was determined as the K_{off}/K_{on} ratio.

NMR Spectroscopy. NMR data were acquired at 25 °C on either a Bruker Avance AV700 or a Bruker Avance AV600 spectrometer (Bruker, Fällanden, Switzerland) equipped with a cryoprobe accessory. Uniformly ^{15}N- and ^{15}N/^{13}C-labeled proteins were prepared in NMR buffer (90% H_2O/10% D_2O, 20 mM phosphate, 50 mM NaCl, 1 mM DTT, 0.01% NaN_3, pH 6.5). Backbone resonance assignments of free Bcl-X_L were achieved by using data from 2D ^{1}H−^{15}N HSQC, 3D HNCACB, CBCACONH, HNCA, and HN(CO)CA. The chemical shift perturbations were monitored by 2D ^{1}H−^{15}N heteronuclear single-quantum correlation (HSQC) spectroscopy upon the addition of different amounts of ligands. The weighted chemical shift perturbations were calculated by the equation $\Delta CS = (\Delta^1H^2 + (0.154\Delta^{15}N)^2)^{0.5}$, in which Δ^1H and Δ^{15}N are the chemical shift changes on the ^{1}H and ^{15}N dimensions (*21*). Residual dipolar coupling (RDC) measurements were achieved by adding 16 mg/mL Pf1 filamentous phage from ASLA (Riga, Latvia) to ^{15}N-labeled Bcl-X_L/unlabeled SN15 peptide. The one-bond ^{1}H−^{15}N couplings for isotropic and aligned samples were measured using ^{15}N-IPAP-HSQC experiments. NMR data were processed and analyzed on Linux workstations using Topspin 1.3 (Bruker), NMRPipe (*22*), and Sparky (*23*).

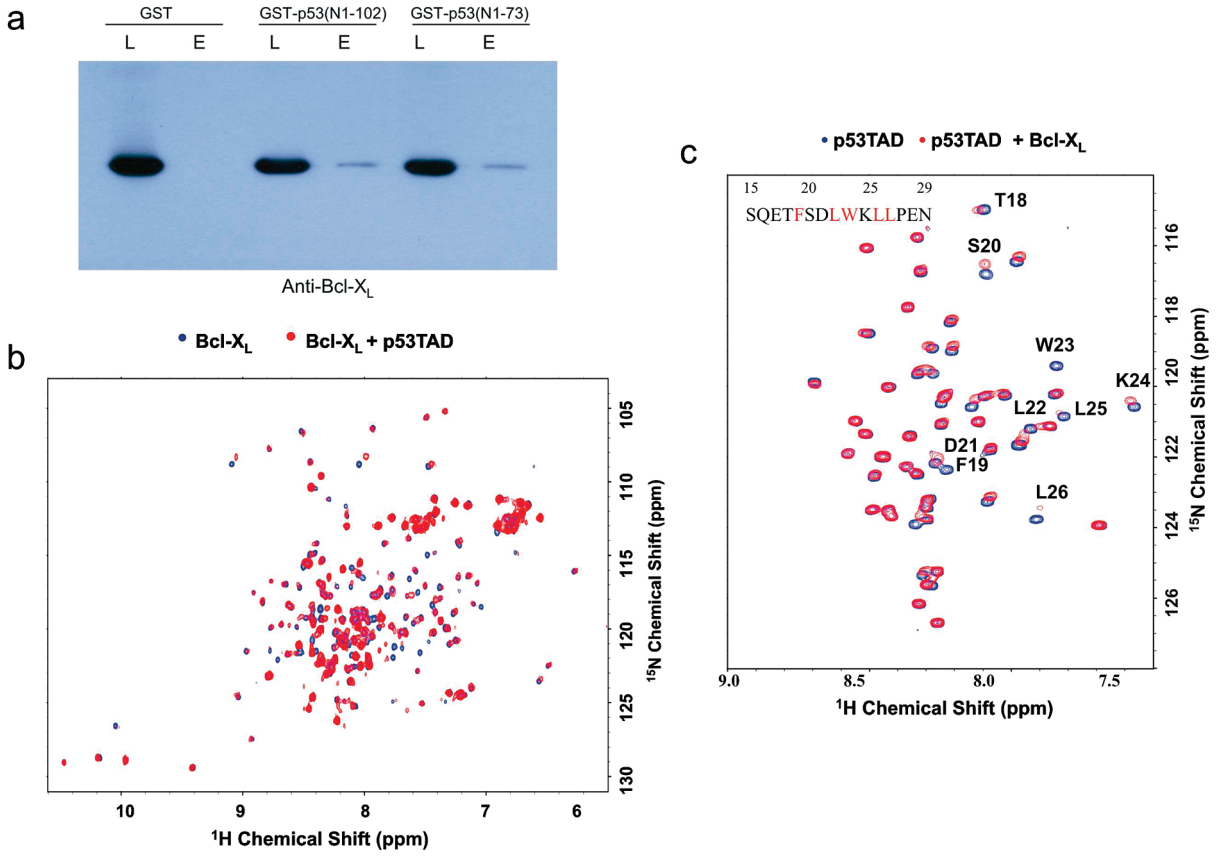

FIGURE 1: Interaction between p53TAD and Bcl-X_L. (a) Comparison of Bcl-X_L/p53NTD and Bcl-X_L/p53TAD interactions using a GST pull-down assay. GST was used as a control. Loaded and eluted samples of GST beads were analyzed by Western blot using the anti-Bcl-X_L antibody. (b) Bcl-X_L was uniformly ^{15}N-labeled and monitored on 2D ^{1}H−^{15}N HSQC spectra upon the addition of unlabeled p53TAD. Shown is an overlaid HSQC spectrum recorded on ^{15}N-labeled Bcl-X_L in the absence (blue) or presence (red) of unlabeled p53TAD. (c) 2D ^{1}H−^{15}N HSQC spectra of ^{15}N-labeled p53TAD in the absence (blue) and presence (red) of unlabeled Bcl-X_L were overlaid. 0.2 mM p53TAD and 0.2 mM Bcl-X_L were used in the experiments. The residues showing obvious chemical shift perturbations are indicated by residue number. The residues showing extensive line broadening are highlighted in red in the SN15 peptide sequence.

Structural Determination of SN15 Peptide by NMR Spectroscopy. NMR experiments to determine the structures of the peptide SN15 in the free and bound state with Bcl-X_L were carried out on a Bruker Avance AV700 equipped with a cryoprobe. Two-dimensional transferred NOE experiments (*24*) of 6 mM SN15 were conducted at 25 °C with mixing times between 100 and 200 ms in the presence of 0.5 mM Bcl-X_L. The resonance assignment of the unlabeled 2 mM free peptide SN15 was obtained manually through a standard assignment procedure using homonuclear proton experiments: first, the total correlation spectroscopy (TOCSY) was collected to identify individual spin systems; then the rotating-frame Overhauser effect spectroscopy (ROESY) experiment was employed to link amino acids in the sequence and provide distance restrains. Mixing times of 100 ms for TOCSY and 100−300 ms for ROESY were used to record data. Spectra were processed by Topspin 1.3 and Felix (Accelrys, San Diego, CA) and analyzed using NMRView (*25*). The ensembles of the SN15 structures in the free state and bound state with Bcl-X_L were calculated with CYANA (*26*, *27*), based on both manually and automatically assigned NOEs. From the ROESY experiment of free SN15, there were a total of 210 peaks picked. Among them, 128 peaks were manually assigned and kept unchanged for the structure calculation, while the rest of the peaks were automatically analyzed by the CYANA program during the structure calculation in an iterative manner (*26*, *27*). A total of 118 distance restraints were derived from the assignments and used for the determination of the free SN15 conformation. Similarly, in the transferred NOE experiment of SN15 in the bound state, a total of 385 peaks were picked. Among them, 254 peaks were manually assigned and kept unchanged, and the rest of the peaks were automatically interpreted by the CYANA program, which totally produced 259 distance restraints to calculate the final SN15 structure in the bound state. The final 20 energy-minimized structures with the lowest target function energy were selected for further analysis. The structures were visualized by PyMOL (*28*) and SwissPDB viewer (*29*).

Bcl-X_L/SN15 Complex Structural Model. The model of the Bcl-X_L/SN15 complex was generated using HADDOCK (*30*). The chemical shift perturbations observed for Bcl-X_L upon complex formation were used to define ambiguous interaction restraints (AIRs). The active site residues of Bcl-X_L were defined as those having chemical shift perturbations larger than the average +0.5 standard deviation or being severely broadened (S110, G138, V141) at the protein to peptide ratio of 1:1 with relative residue-accessible surface area larger than 50% for either side-chain or backbone atoms as calculated with NACCESS (*31*). A total of 101 RDC-based orientation constraints of well-solved residues in the spectra were introduced into structure calculation (data not shown). Starting from the minimized average NMR structure of the Bcl-X_L (PDB ID 1bxl, in complex with Bak BH3 peptide) (*20*) and the SN15 structure calculated in the bound state, 1000 rigid-body solutions were generated. The best 200 solutions were selected for semiflexible refinement and finally refined in explicit water. The clustering was performed using

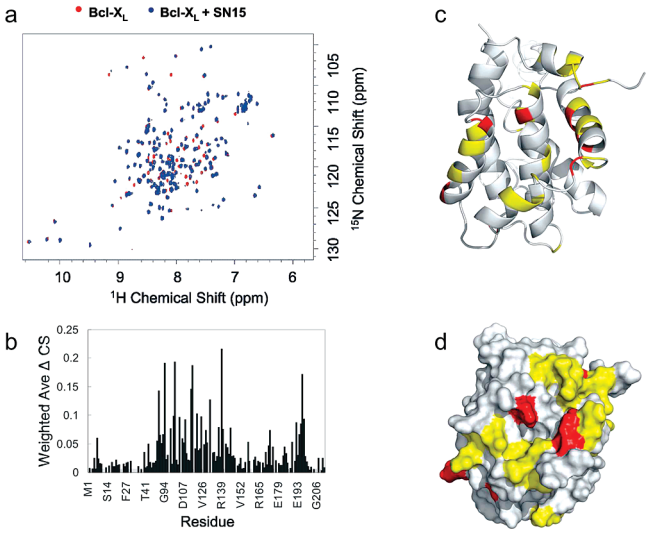

FIGURE 2: Interaction between Bcl-X_L and SN15. (a) ^{1}H−^{15}N HSQC spectra of the Bcl-X_L in the absence (red) and presence (blue) of the SN15 peptide. The 0.2 mM Bcl-X_L and 0.2 mM SN15 peptide were used in the experiments. (b) Chemical shift changes in the Bcl-X_L residues upon binding to the SN15 peptide. Chemical shift perturbation data were calculated at an equal molar ratio of SN15 to the Bcl-X_L. (c) Ribbon and (d) surface representation of Bcl-X_L to indicate SN15 interaction on Bcl-X_L. Amino acids showing chemical shift perturbations upon the addition of the SN15 peptide were displayed in yellow and red: yellow, 0.05 < ΔCS < 0.1; red, ΔCS > 0.1.

a 1.7 Å cutoff. The 20 lowest energy structures in the lowest energy cluster were accepted as the best representatives of the complex.

RESULTS

p53TAD/Bcl-X_L Interaction. The p53NTD (residues 1−102) contributes to the formation of the p53/Bcl-X_L complex (*19*) and includes a transcription activation domain (residues 1−73) and proline-rich domain. To determine whether both of these domains are necessary for the interaction, the proline-rich domain was truncated from p53NTD to leave p53TAD alone. Both p53NTD and p53TAD were observed to interact with Bcl-X_L (Figure 1), showing that the Bcl-X_L protein levels in eluted fractions from GST-p53NTD and GST-p53TAD columns were similar, indicating GST-p53NTD and GST-p53TAD bind to Bcl-X_L with similar binding affinity and the proline-rich domain of p53 may be dispensable for the binding with Bcl-X_L. The molecular interaction was further confirmed by observing the chemical shift perturbations on a 2D ^{1}H−^{15}N HSQC spectrum of the ^{15}N-labeled Bcl-X_L in the presence of unlabeled p53TAD. Obvious chemical shift changes were detected in some amino acids upon binding (Figure 1b). On the other hand, to monitor the binding site on p53TAD, we performed a 2D ^{1}H−^{15}N HSQC NMR experiment using uniformly ^{15}N-labeled p53TAD. The overlay of the spectra recorded in the presence and absence of Bcl-X_L showed no major conformational change in p53TAD. However, the differential line broadening of some of the residues

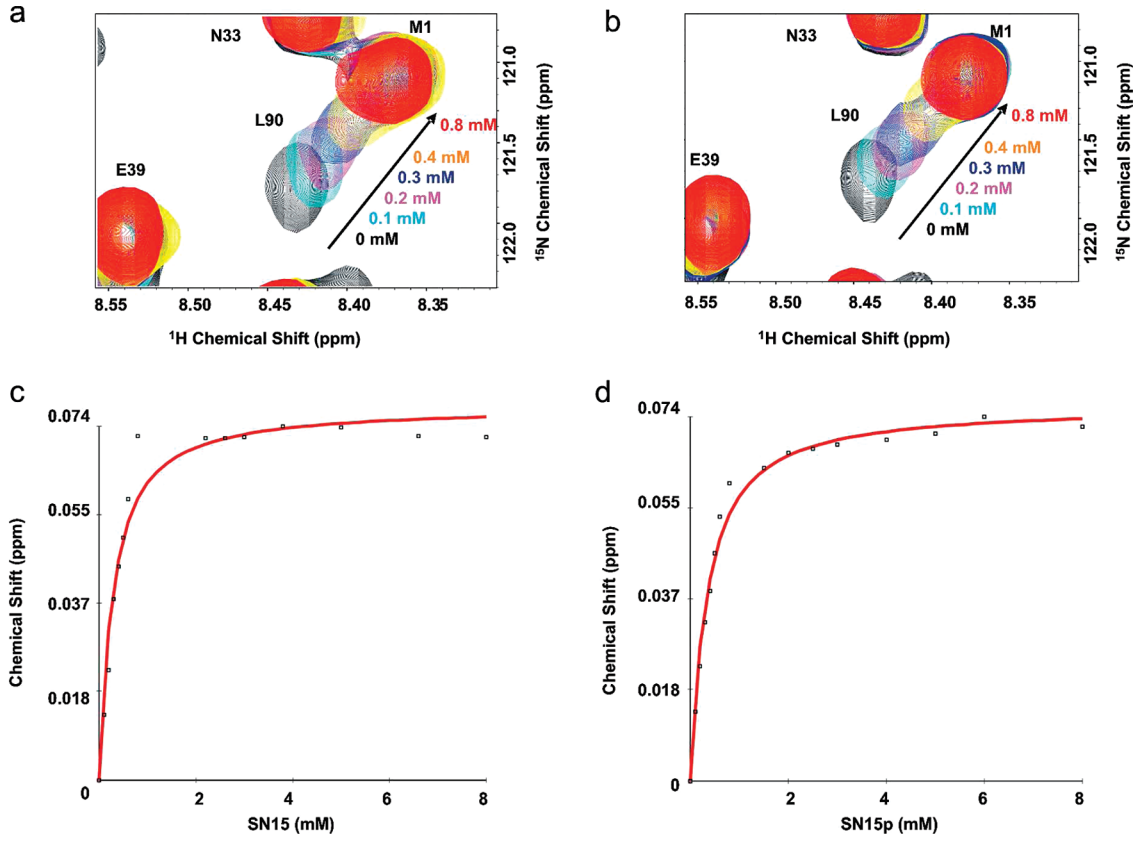

FIGURE 3: Sections of the 2D ^{1}H−^{15}N HSQC spectra of ^{15}N-labeled Bcl-X_L (0.1 mM) upon titration with peptides SN15 (a) and SN15p (b) [0 mM (black), 0.1 mM (cyan), 0.2 mM (magenta), 0.3 mM (blue), 0.4 mM (yellow) and 0.8 mM (red)]. Binding curves are shown for the titration of Bcl-X_L with peptides SN15 (c) and SN15p (d). The chemical shift values were calculated by averaging the weighted individual chemical shifts of three residues, L90, E92, and E124, located close to the binding pocket. The binding curve fits were generated with a single-site binding model using the nonlinear least-squares method. The determined dissociation constants (K_d), 0.26 mM (SN15) and 0.33 mM (SN15p), were the average of the K_d values of the three residues, calculated by fitting the binding curve of each residue.

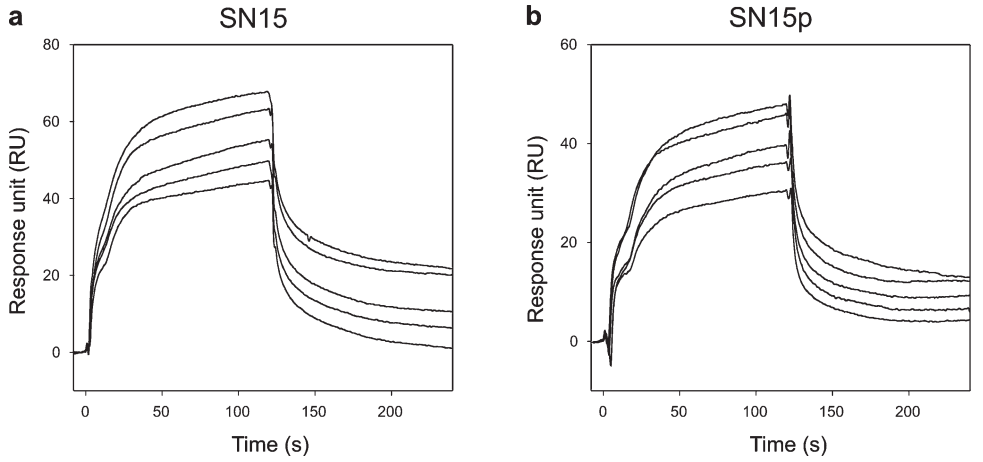

FIGURE 4: Surface plasma resonance analysis for the binding of Bcl-X_L with the SN15 peptide. Surface plasma resonance data were recorded on a BIAcore 3000 with Bcl-X_L immobilized to a channel of the CM5 sensor chip and peptide concentrations at 0.625, 1.25, 2.5, 5, and 10 μM. Surface plasma resonance sensorgrams are shown for the binding of Bcl-X_L with the wild-type SN15 peptide (a) and the phosphorylated SN15 peptide (b).

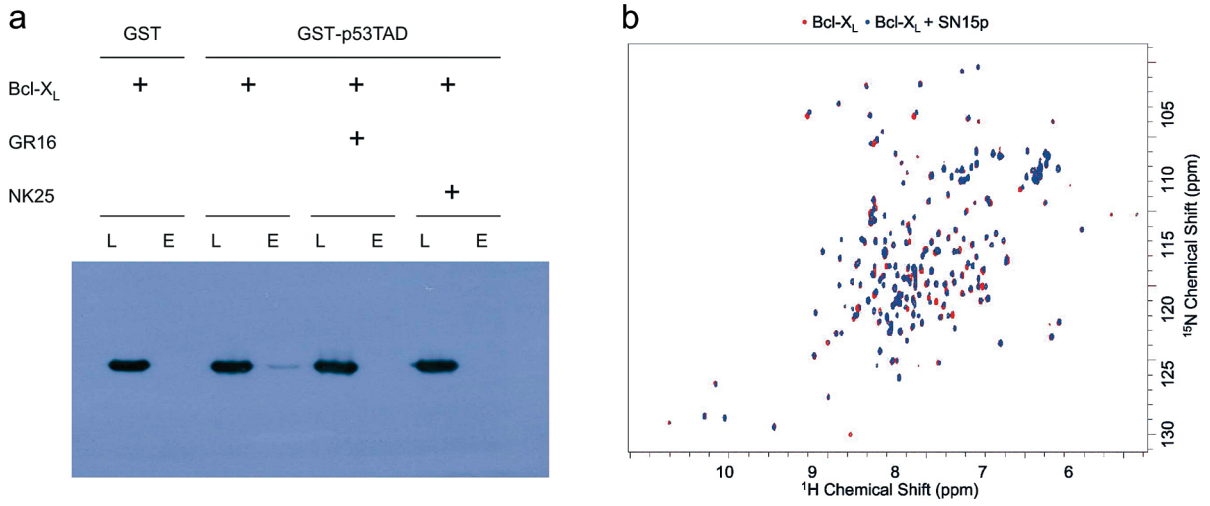

FIGURE 5: (a) BH3 peptides compete with p53TAD from the Bcl-X_L/p53TAD complex. A GST pull-down assay was performed using GST-p53TAD with the Bcl-X_L protein in the absence or presence of the GR16 peptide (from the Bak BH3 domain) or the NK25 peptide (from the Bad BH3 domain). GST was used as a control. Loaded and eluted samples were analyzed by Western blot using an anti-Bcl-X_L antibody. (b) Phosphorylation of T18 on p53 does not affect Bcl-X_L/p53TAD interaction. Shown is an overlaid 2D $^1H-^{15}N$ HSQC spectrum recorded using ^{15}N-labeled Bcl-X_L in the absence of the T18-phosphorylated peptide (SN15p) (red) and presence of SN15p (blue).

was observed. F19, L22, W23, L25, and L26 were the most severely broadened (Figure 1c, residues highlighted in red) due to an exchange between the two sites on an intermediate time scale, suggesting that these residues are located in the binding site. The majority of the amino acids perturbed upon binding Bcl-X_L were located in a specific region in p53TAD (from S15 to N29), which is also the binding site of p53 with its negative regulator MDM2 (*32*, *33*), suggesting that p53TAD/Bcl-X_L shares the same binding site on the p53TAD as p53/MDM2.

SN15/Bcl-X_L Interaction. The NMR study results prompted us to further define the detailed molecular interaction between p53TAD and Bcl-X_L. For this, we used the SN15 peptide that contained residues from S15 to N29 of p53. After adding the SN15 peptide, significant chemical shift changes were detected on the 2D $^1H-^{15}N$ HSQC spectrum of ^{15}N-labeled Bcl-X_L, suggesting the binding between the protein and the ligand (Figure 2a,b). Most of the amino acids involved in the binding are located in the BH1, BH2, and BH3 regions and the α3 and α4 helices between BH3 and BH1 (Figure 2c,d). Binding affinity (K_d) of the SN15 peptide to Bcl-X_L was determined by measuring the chemical shift changes as a function of ligand concentration, until Bcl-X_L is fully saturated with the peptide (Figure 3a). The data were fitted by a least-squares grid search, assuming a single-site binding model. Along with the increase in the SN15 concentration, some peaks showed chemical shift perturbations, while others disappeared from the spectrum, indicating that the complex is in fast to intermediate exchange on NMR time scale and suffers substantial line broadening for the majority of interfacial resonances. The determined binding constant was 0.26 ± 0.06 mM, which represents the average values of three residues (L90, E92, E124) located close to the binding pocket. Interestingly, the K_d of the SN15 peptide to immobilized Bcl-X_L determined by surface plasmon resonance was 2.2 μM (Figure 4a). The difference on the K_d values may be due to different techniques and test conditions *in vitro*.

Bcl-X_L is an important antiapoptotic member of the Bcl-2 family proteins. The heterodimerization between the Bcl-2 family proteins plays a critical role in the regulation of apoptosis (*34*). The BH3 region of the proapoptotic proteins such as Bak and Bad interacts with Bcl-X_L on its hydrophobic groove consisting of the BH1, BH2, and BH3 domains of Bcl-X_L (*20*, *35*). The Bcl-X_L/Bak BH3 peptide complex structure showed that the Bak

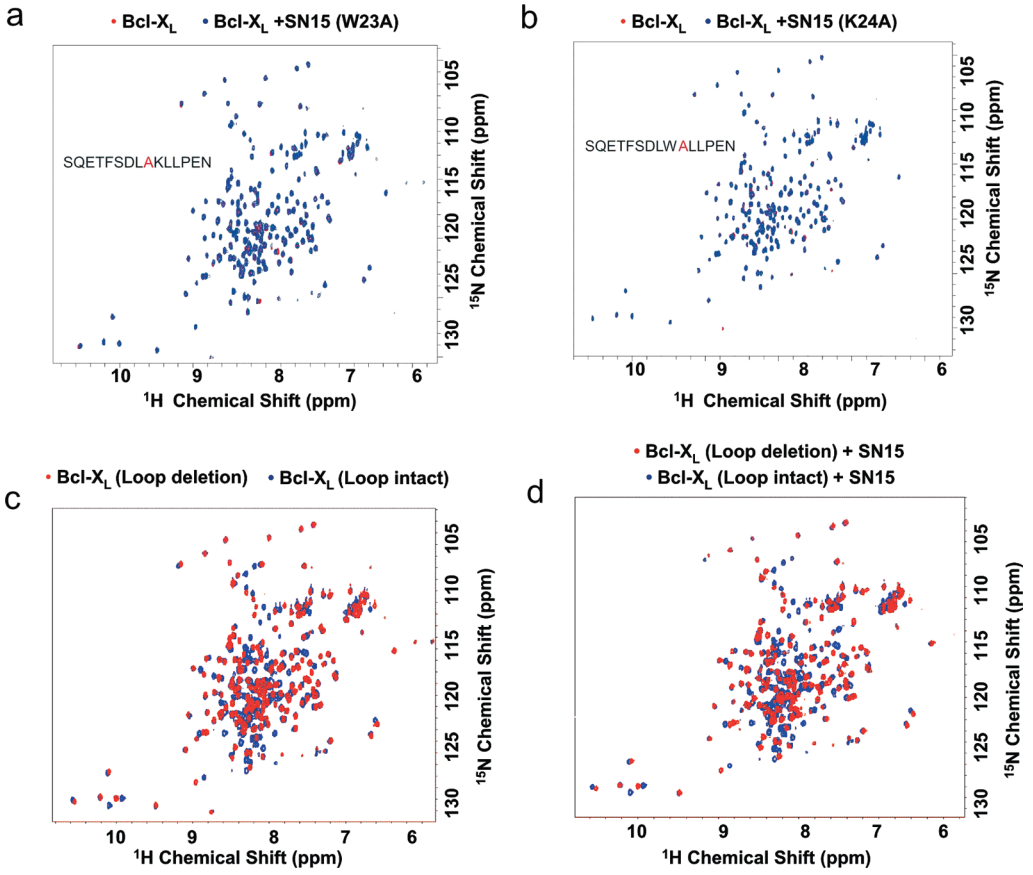

FIGURE 6: The identification of key residues in p53TAD critical for its binding to Bcl-X_L and the role of the flexible loop of Bcl-X_L on the molecular interaction. Shown is a 2D $^{1}H-^{15}N$ HSQC spectrum recorded on ^{15}N-labeled Bcl-X_L in the absence (red) or presence (blue) of the SN15W23A peptide (a). Shown is a 2D $^{1}H-^{15}N$ HSQC spectrum recorded on ^{15}N-labeled Bcl-X_L in the absence (red) or presence (blue) of the SN15 K24A peptide (b). (c) 2D $^{1}H-^{15}N$ HSQC spectra recorded on ^{15}N-labeled loop deletion Bcl-X_L (red) and ^{15}N-labeled loop intact Bcl-X_L (blue) in the absence of the SN15 peptide. (d) 2D $^{1}H-^{15}N$ HSQC spectra recorded on ^{15}N-labeled loop deletion Bcl-X_L (red) and ^{15}N-labeled loop intact Bcl-X_L (blue) in the presence of the SN15 peptide.

BH3 peptide adopts an amphipathic α-helix binding to this groove through hydrophobic and electrostatic interactions (*20*). Our data showed that this region is also involved in the Bcl-X_L/SN15 interaction, indicating that the binding pattern of Bcl-X_L/SN15 might be similar to that of Bcl-X_L/Bak BH3. To delineate the molecular basis of the Bcl-X_L/SN15 interaction, we first performed a competition binding assay using the BH3 peptides from Bak (GR16) and Bad (NK25). As seen in Figure 5a, the p53TAD/Bcl-X_L interaction was abolished in the presence of the GR16 or NK25 peptides, confirming that the BH3 peptides compete with SN15 to bind to Bcl-X_L. The results suggest that SN15 and BH3 peptides share a common binding site on Bcl-X_L.

The SN15 peptide contains several phosphorylation sites, such as S15, T18, and S20. Among these, the phosphorylation of T18 significantly weakens p53/MDM2 binding and p53 stability (*36*, *37*). To test whether the formation of a complex between p53 and Bcl-X_L employs the same regulatory mechanism as the p53/MDM2 complex, a T18-phosphorylated SN15 (SN15p) was prepared and tested for its binding to Bcl-X_L (Figure 5b). Our NMR data showed that in the presence of the SN15p the chemical shift perturbations on the ^{15}N-labeled Bcl-X_L spectrum were similar to those observed upon adding the SN15 peptide. The K_d of the SN15p peptide to Bcl-X_L determined by NMR spectroscopy was 0.33 ± 0.09 mM (Figure 3b,d), whereas the K_d of the SN15p peptide to immobilized Bcl-X_L determined by surface plasmon resonance was 4.1 μM (Figure 4b), which are similar to the values of SN15/Bcl-X_L complex formation (Figures 3a,c and 4a). This indicates that, unlike MDM2, the phosphorylation of T18 affects little the binding of SN15 to Bcl-X_L. Taken together, these results suggest that Bcl-X_L and MDM2 have the common binding site on p53TAD but have a different binding pattern for the phosphorylated peptide. An alanine scanning mutational study on the SN15 peptide was performed as an attempt to identify which amino acids are critical to the Bcl-X_L and SN15 peptide binding. A 15-member SN15 peptide library was produced with each peptide containing a single residue changed to alanine. The Bcl-X_L binding abilities of the alanine mutants were analyzed on 2D $^{1}H-^{15}N$ HSQC spectra of ^{15}N-labeled Bcl-X_L in the presence of the mutant peptides. Among the mutant peptides, the peptides SN15W23A and SN15K24A showed little chemical shift perturbations on Bcl-X_L, thus suggesting that W23 and K24 are critical ones for the interaction (Figure 6a,b).

In our study for the molecular interaction between Bcl-X_L and the SN15 peptide, Bcl-X_LΔTMΔloop, in which the C-terminal transmembrane region and the loop region from M45 to A84 are truncated, was used. To check whether the flexible loop region of Bcl-X_L influences the Bcl-X_L/SN15 interaction, Bcl-X_LΔTM (loop intact construct) and its interaction with the SN15 peptide were also examined on 2D $^{1}H-^{15}N$ HSQC NMR experiments (Figure 6c,d), showing that the binding pattern of Bcl-X_LΔTM/SN15 is similar to that of the Bcl-X_LΔTMΔloop/SN15. The chemical shifts of the residues from the loop region, which are shown as extra blue peaks located mainly in the central part of the

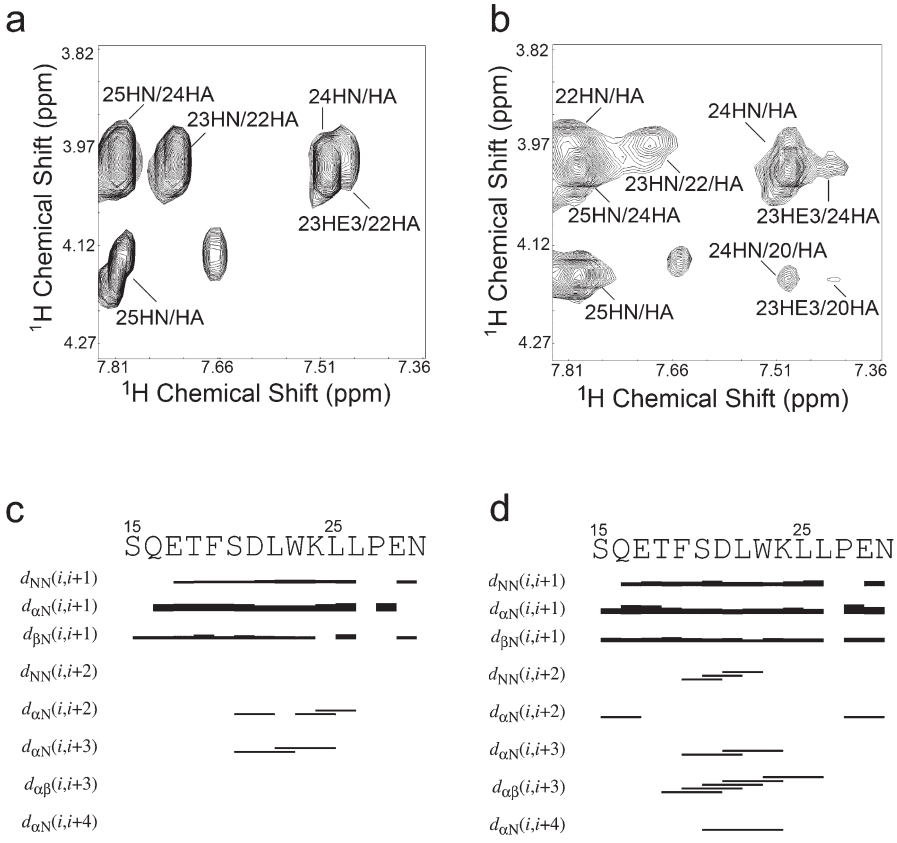

FIGURE 7: NOE data show the differences of the SN15 peptide structure in the absence and presence of Bcl-X_L. (a) The 2D $^1H-^1H$ ROESY spectrum recorded with a mixing time of 200 ms shows NOEs in the amide/aliphatic fingerprint for the free peptide. (b) As a comparison, the 2D $^1H-^1H$ transferred NOESY spectrum recorded with a mixing time of 200 ms shows NOEs in the same region for the peptide in the presence of Bcl-X_L. (c, d) A summary of the short- and medium-range NOEs for SN15 in the absence and presence of Bcl-X_L shows the differences of the SN15 peptide structure upon binding to Bcl-X_L. The thickness of the bar presents the relative intensity (i.e., strong, medium, or weak) of the NOEs.

spectrum, basically remained unchanged upon the addition of the SN15 peptide, indicating that the flexible loop of Bcl-X_L may not play an important role in the molecular interaction between Bcl-X_L and the SN15 peptide.

Structure of the SN15 Peptide and SN15/Bcl-X_L Complex Structural Model. In the native p53 conformation the region p53TAD is disordered (*38*). However, it is not completely unstructured; it possesses local structural elements: α-helix and turns. The SN15 peptide contains the α-helix that is one of the structural elements present in p53TAD. The chemical shift changes seen on the SN15 residues of p53TAD when binding to Bcl-X_L indicate that a minor conformational change may occur to SN15. To verify the finding, we have determined the structures of SN15 in free and complex states, respectively. More short- and medium-range NOEs were observed in the SN15 peptide when binding to Bcl-X_L (Figure 7). The structure of SN15 complexed with Bcl-X_L was determined from a total of 259 NMR-derived distance restraints. The average root-mean-square deviation (RMSD) values for all of the residues of the free and bound states of SN15 were 1.49 and 0.23 Å for the backbone atoms and 2.47 and 0.80 Å for the heavy atoms, respectively (Table 1). Together with other structural statistics data and NOE plots (Figure 7c,d), these suggest that the SN15 peptide undergoes a conformational change and adopts a more stable structure with an extended α-helix to bind with Bcl-X_L (Figure 8a,b).

As the Bcl-X_L/SN15 complex is in the fast to intermediate exchange on the NMR chemical shift time scale and suffers substantial line broadening for the majority of interfacial resonances, it is difficult to extract unambiguous intermolecular NOEs between the Bcl-X_L binding pocket and SN15 peptide with isotope-filtered NOESY experiments. This is consistent with

Table 1: Structural Statistics for SN15 Alone (Free) and in Complex with Bcl-X_L (Bound)[a]

	free	bound
distance restraints	118	259
intraresidual ($i = j$)	58	78
sequential ($\|i - j\| = 1$)	46	105
medium range ($1 < \|i - j\| < 5$)	14	76
long range ($\|i - j\| > 4$)	0	0
dihedral angle restraints (Φ and Ψ)	14	16
total no. of restraint violations > 0.1 Å	1	0
total no. of dihedral angle violations > 5°	0	0
Ramachandran plot (% of all residues)		
most favored regions	86.70	91.20
additionally allowed regions	13.30	8.80
generously allowed regions	0.00	0.00
disallowed regions	0.00	0.00
av RMSD (Å) to mean for top 20 structures (all residues)		
backbone atom	1.49 ± 0.34	0.23 ± 0.08
heavy atom	2.47 ± 0.39	0.80 ± 0.10

[a]The ensemble for bound SN15 contained no NOE violation greater than 0.1 Å and no dihedral angle violation greater than 5°. The average root-mean-square deviation (RMSD) values for bound SN15 were determined to be 0.23 Å for the backbone atoms and 0.80 Å for heavy atoms residues, respectively. Structural quality of the NMR ensemble was analyzed using PROCHECK showing that 91.2% of the residues of the bound SN15 in the most favored and 8.8% in the additionally allowed regions of the Ramachandran plot.

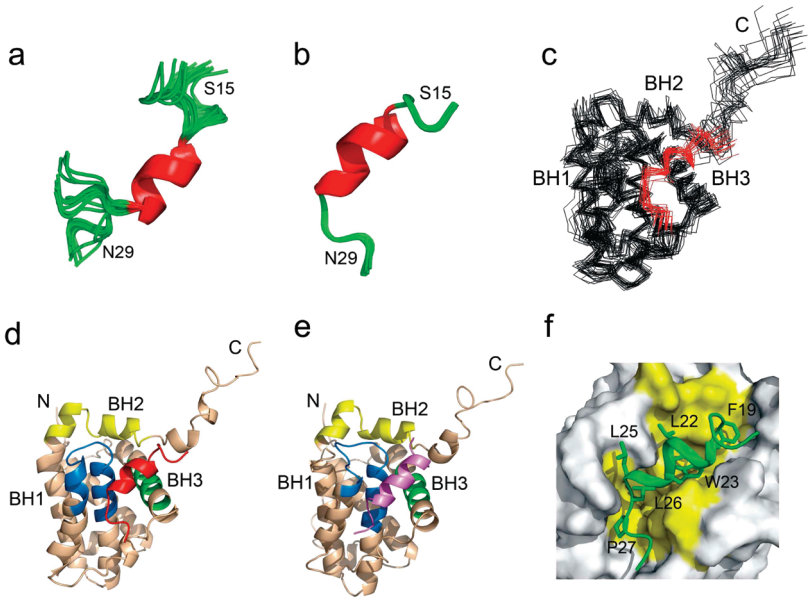

FIGURE 8: NMR structures of SN15 and the model of the Bcl-X_L/SN15 complex. (a) Ensemble of the top 20 NMR-derived structures of the free SN15 peptide. (b) Ensemble of the top 20 NMR-derived SN15 structures in the presence of Bcl-X_L. (c) The model of the Bcl-X_L (in black) complexed with the SN15 (in red) built by NMR-based docking is shown as the backbone. (d) Ribbon depiction of the complex model. The BH1, BH2, and BH3 regions of Bcl-X_L are shown in blue, yellow, and green, respectively, and SN15 is shown in red. (e) The NMR structure of the Bcl-X_L/Bak complex is shown as a comparison (PDB ID 1bxl), where Bak is colored in pink. (f) Surface representation of the hydrophobic pocket of Bcl-X_L bound to the SN15 peptide. The hydrophobic residues of Bcl-X_L are colored in yellow, and the SN15 peptide is shown in green. Hydrophobic residues of SN15 are labeled in black.

previous observations for other complexes in the intermediate exchange regime (*39*, *40*). Based on the NMR structure of the SN15 peptide in the bound state, 101 RDC restraints, and the binding site information on Bcl-X_L provided by the NMR experiments, a Bcl-X_L/SN15 complex structure model was proposed. Experimentally measured RDCs were in agreement with the back-calculated RDC values from the Bcl-X_L structure in the complex model (data not shown). The model showed that the peptide with an extended α-helix induced upon binding with Bcl-X_L interacts with the hydrophobic pocket formed by the BH1, BH2, and BH3 regions (Figure 8c−d), which is similar to the pattern of the Bcl-X_L/Bak BH3 peptide interaction (Figure 8e). Like the BH3 peptide, the hydrophobic side chains (F19, L22, W23, L25, L26, and P27) of the SN15 peptide are directed into the hydrophobic cleft of Bcl-X_L (Figure 8f). This similarity suggests that BH3 peptides would have a higher binding affinity with Bcl-X_L compared to that of SN15 with Bcl-X_L as the BH3 peptides were able to abolish the Bcl-X_L/SN15 interaction. In our structural models, SN15 and Bak peptides show similar binding modes with Bcl-X_L in the hydrophobic groove on the surface but are opposite in the directional sense.

DISCUSSION

Recently, there has been an increasing number of reports on the transcription-independent mechanism of p53 (*41*, *42*). The interactions between p53 and several Bcl-2 family proteins, such as Bcl-2, Bcl-X_L, Bax, Bak, Bad, and PUMA, have been identified as playing important roles in this pathway (*12*−*14*, *16*, *18*). It is possible that p53 affects the balance between anti- and pro-apoptotic Bcl-2 family proteins by forming complexes, thus inducing the permeability of the outer mitochondrial membrane. However, the detailed mechanism remains unclear. Thus, it would be interesting and important to understand the interaction between p53 and the Bcl-2 family proteins at the molecular level.

Bcl-2 and Bcl-X_L were the first Bcl-2 family proteins reported to bind to p53 (*12*). The p53/Bcl-X_L complex formation directly induces the permeabilization of the mitochondrial membrane and results in apoptosis. Initial studies showed that the p53DBD binds to Bcl-X_L. However, Chipuk et al. reported that p53NTD, which includes p53TAD and the proline-rich domain, is necessary and sufficient to induce transcription-independent apoptosis, whereas the DNA-binding domain is dispensable (*18*). More interestingly, it is also reported that p53 can be cleaved through a caspase-dependent pathway. Two out of the four generated fragments of p53, p53-(1−186) and p53-(22−186), which contain the N-terminal domain and part of the DNA-binding domain, translocate to the mitochondria and induce apoptosis in the absence of transcriptional activity (*43*). In this study we demonstrated that the proline-rich domain is dispensable for p53NTD/Bcl-X_L interaction *in vitro*, suggesting that the proline-rich domain may regulate the transcription-independent proapoptotic activity of p53 through other mechanisms that await further investigation.

Free p53TAD was reported to possess local structural elements including α-helix and turns. In our present study, we have observed that, on a 2D $^{1}H-^{15}N$ HSQC spectrum using ^{15}N-labeled p53TAD in the presence of Bcl-X_L, no major conformational changes were observed in p53TAD upon binding to Bcl-X_L. However, the differential line broadening of certain residues was observed. F19, L22, W23, L25, and L26 were the most severely broadened due to an exchange between two sites on an intermediate time scale (Figure 1c). The majority of the amino acids involved are located in a selected region in p53TAD, from S15 to N29, indicating that the hydrophobic residues located in the SN15 of p53TAD are directly involved in the molecular interaction with Bcl-X_L . It is interesting that this SN15 region is also the binding site for MDM2 (*33*).

Previous studies on the interaction between p53DBD and Bcl-X_L indicated that a loop from the p53 DNA-binding domain

made up of residues 239−248 interacts with a groove on Bcl-X_L that is formed by the C-terminus of α1 and part of the α3/α4 and α5/α6 loops (*12*, *17*). In this study we showed that the SN15 from p53TAD binds to the hydrophobic pocket of Bcl-X_L. The binding interface on Bcl-X_L contains BH1, BH2, and BH3 domains and the α3 and α4 helices between BH3 and BH1, suggesting that p53DBD and p53TAD have different binding sites on Bcl-X_L. Recently, the interaction between p53NTD with Bcl-X_L was also examined using a fluorescence anisotropy-based assay (*44*), showing no obvious interaction between p53NTD and Bcl-X_L. In our previous study we showed the molecular interaction between p53NTD and Bcl-X_L using fluorescence resonance energy transfer (FRET) in cells and NMR spectroscopy approaches *in vitro* (*19*). So it is possible that the discrepancy observed in the molecular interactions might be due to different experimental conditions. Our SN15 peptide mutagenesis experiments identified critical residues responsible for the interaction between SN15 and Bcl-X_L, suggesting that the interaction detected in our studies is not due to nonspecific bindings.

The negative regulatory activity of MDM2 is important for p53 to control its protein level and activity in normal cells. MDM2 binds to p53 on its transactivation domain to inhibit its activity and induce its degradation. When cells receive death signals, p53 needs to be activated and bypasses MDM2-dependent degradation by its posttranslation modification (*1*, *3*). The phosphorylation of T18 on p53 is reported to inhibit the p53/MDM2 interaction (*37*). However, in our study we showed that the pT18 is not critical for binding to Bcl-X_L. It is reasonable to assume that p53 is stabilized by phosphorylation on T18, thus bypassing the MDM2 binding, but is still able to bind to Bcl-X_L to execute its mitochondrial apoptotic activity. SN15 contains an α-helix when binding to MDM2 (*33*). Similarly, SN15 binds to Bcl-X_L with conformational change accompanied by an extended and better defined α-helix. The proposed complex structural model suggests that SN15 adopts an α-helix to interact with the hydrophobic pocket of Bcl-X_L. This pattern is similar to that of the Bcl-X_L/Bak BH3 peptide complex (*20*). The Bak peptide binds to the hydrophobic pocket with the hydrophobic side chains of the peptide (V74, L78, I81, and I85) pointing into the hydrophobic pocket of Bcl-X_L and stabilizing complex formation. Similarly, in the complex model of Bcl-X_L/SN15 (Figure 8f), the side chains of the hydrophobic amino acids (F19, L22, W23, L25, L26, and P27) of the SN15 face the Bcl-X_L hydrophobic pocket. In the Bcl-X_L/Bak complex, in addition to the hydrophobic interactions, the electrostatic interactions between Bak peptide (Arg76, Asp83, and Asp84) and Bcl-X_L (Glu129, Arg139, and Arg100) also play an important role in stabilizing the complex formation. In our study, the SN15K24A mutant peptide showed loss of binding with Bcl-X_L (Figure 6b). However, in our complex structural model of Bcl-X_L/SN15, K24 does not make direct contacts with any negatively charged residues. This suggests that no electrostatic interaction is involved in the molecular interaction between the SN15 peptide and Bcl-X_L. The loss of the binding affinity between the SN15K24A mutant peptide and Bcl-X_L might be attributable to the loss of secondary structure through the mutation. The hydrophobic interaction appears to be the primary stabilizing force in the complex formation. This also explains why the binding affinity of Bcl-X_L/SN15 is much lower than that of Bcl-X_L/Bak.

In conclusion, this study provides insightful information for the elucidation of the interaction between p53 and Bcl-X_L and other Bcl-2 family proteins and the roles they play in the p53-mediated transcription-independent apoptotic mechanisms. We presented that the MDM2-binding region of p53 provides a binding site for Bcl-X_L, and the mode of the binding is similar to that of Bcl-X_L and BH3 peptides of proapoptotic proteins. The interaction between p53 and the Bcl-2 family proteins has aroused much interest for its critical role in the transcription-independent mechanism of p53 in response to apoptotic stimuli. Further studies are necessary to determine if this is a universal mechanism for p53 interaction with other Bcl-2 family proteins.

REFERENCES

1. Vousden, K. H., and Lu, X. (2002) Live or let die: the cell's response to p53. *Nat. Rev. Cancer 2*, 594–604.
2. Hollstein, M., Sidransky, D., Vogelstein, B., and Harris, C. C. (1991) p53 mutations in human cancers. *Science 253*, 49–53.
3. Vogelstein, B., Lane, D., and Levine, A. J. (2000) Surfing the p53 network. *Nature 408*, 307–310.
4. Haupt, Y., Rowan, S., Shaulian, E., Vousden, K. H., and Oren, M. (1995) Induction of apoptosis in HeLa cells by trans-activation-deficient p53. *Genes Dev. 9*, 2170–2183.
5. Kokontis, J. M., Wagner, A. J., O'Leary, M., Liao, S., and Hay, N. (2001) A transcriptional activation function of p53 is dispensable for and inhibitory of its apoptotic function. *Oncogene 20*, 659–668.
6. Caelles, C., Helmberg, A., and Karin, M. (1994) p53-dependent apoptosis in the absence of transcriptional activation of p53-target genes. *Nature 370*, 220–223.
7. Wagner, A. J., Kokontis, J. M., and Hay, N. (1994) Myc-mediated apoptosis requires wild-type p53 in a manner independent of cell cycle arrest and the ability of p53 to induce p21waf1/cip1. *Genes Dev. 8*, 2817–2830.
8. Yan, Y., Shay, J. W., Wright, W. E., and Mumby, M. C. (1997) Inhibition of protein phosphatase activity induces p53-dependent apoptosis in the absence of p53 transactivation. *J. Biol. Chem. 272*, 15220–15226.
9. Schuler, M., and Green, D. R. (2001) Mechanisms of p53-dependent apoptosis. *Biochem. Soc. Trans. 29*, 684–688.
10. Marchenko, N. D., Zaika, A., and Moll, U. M. (2000) Death signal-induced localization of p53 protein to mitochondria. A potential role in apoptotic signaling. *J. Biol. Chem. 275*, 16202–16212.
11. Talos, F., Petrenko, O., Mena, P., and Moll, U. M. (2005) Mitochondrially targeted p53 has tumor suppressor activities in vivo. *Cancer Res. 65*, 9971–9981.
12. Mihara, M., Erster, S., Zaika, A., Petrenko, O., Chittenden, T., Pancoska, P., and Moll, U. M. (2003) p53 has a direct apoptogenic role at the mitochondria. *Mol. Cell 11*, 577–590.
13. Leu, J. I., Dumont, P., Hafey, M., Murphy, M. E., and George, D. L. (2004) Mitochondrial p53 activates Bak and causes disruption of a Bak-Mcl1 complex. *Nat. Cell Biol. 6*, 443–450.
14. Chipuk, J. E., Kuwana, T., Bouchier-Hayes, L., Droin, N. M., Newmeyer, D. D., Schuler, M., and Green, D. R. (2004) Direct activation of Bax by p53 mediates mitochondrial membrane permeabilization and apoptosis. *Science 303*, 1010–1014.
15. Chipuk, J. E., Bouchier-Hayes, L., Kuwana, T., Newmeyer, D. D., and Green, D. R. (2005) PUMA couples the nuclear and cytoplasmic proapoptotic function of p53. *Science 309*, 1732–1735.
16. Jiang, P., Du, W., Heese, K., and Wu, M. (2006) The Bad guy cooperates with good cop p53: Bad is transcriptionally up-regulated by p53 and forms a Bad/p53 complex at the mitochondria to induce apoptosis. *Mol. Cell. Biol. 26*, 9071–9082.
17. Petros, A. M., Gunasekera, A., Xu, N., Olejniczak, E. T., and Fesik, S. W. (2004) Defining the p53 DNA-binding domain/Bcl-x(L)-binding interface using NMR. *FEBS Lett. 559*, 171–174.
18. Chipuk, J. E., Maurer, U., Green, D. R., and Schuler, M. (2003) Pharmacologic activation of p53 elicits Bax-dependent apoptosis in the absence of transcription. *Cancer Cell 4*, 371–381.
19. Xu, H., Tai, J., Ye, H., Kang, C. B., and Yoon, H. S. (2006) The N-terminal domain of tumor suppressor p53 is involved in the molecular interaction with the anti-apoptotic protein Bcl-Xl. *Biochem. Biophys. Res. Commun. 341*, 938–944.
20. Sattler, M., Liang, H., Nettesheim, D., Meadows, R. P., Harlan, J. E., Eberstadt, M., Yoon, H. S., Shuker, S. B., Chang, B. S., Minn, A. J., Thompson, C. B., and Fesik, S. W. (1997) Structure of Bcl-xL-Bak peptide complex: recognition between regulators of apoptosis. *Science 275*, 983–986.

21. Seavey, B. R., Farr, E. A., Westler, W. M., and Markley, J. L. (1991) A relational database for sequence-specific protein NMR data. *J. Biomol. NMR 1*, 217–236.
22. Delaglio, F., Grzesiek, S., Vuister, G. W., Zhu, G., Pfeifer, J., and Bax, A. (1995) NMRPipe: a multidimensional spectral processing system based on UNIX pipes. *J. Biomol. NMR 6*, 277–293.
23. Goddard, T. D., and Kneller, D. G. SPARKY 3, University of California, San Francisco.
24. Clore, G. M., and Gronenborn, A. M. (1982) Theory and applications of the transferred nuclear Overhauser effect to the study of the conformations of small ligands bound to proteins. *J. Magn. Reson. 48*, 402–417.
25. Johnson, B. A., and Blevins, R. A. (1994) NMRView: a computer program for the visualization and analysis of NMR data. *J. Biomol. NMR 4*, 603–614.
26. Guntert, P., Mumenthaler, C., and Wuthrich, K. (1997) Torsion angle dynamics for NMR structure calculation with the new program DYANA. *J. Mol. Biol. 273*, 283–298.
27. Guntert, P. (2004) Automated NMR structure calculation with CYANA. *Methods Mol. Biol. 278*, 353–378.
28. DeLano, W. L. (2002) The PyMOL Molecular Graphics System, DeLano Scientific, Palo Alto, CA (http://www.pymol.org).
29. Kaplan, W., and Littlejohn, T. G. (2001) Swiss-PDB Viewer (Deep View). *Briefings Bioinf. 2*, 195–197.
30. Dominguez, C., Boelens, R., and Bonvin, A. M. (2003) HADDOCK: a protein-protein docking approach based on biochemical or biophysical information. *J. Am. Chem. Soc. 125*, 1731–1737.
31. Hubbard, S. J., and Thornton, J. M. (1993) NACCESS Computer Program, Department of Biochemistry and Molecular Biology, University College London, London, U.K.
32. Picksley, S. M., Vojtesek, B., Sparks, A., and Lane, D. P. (1994) Immunochemical analysis of the interaction of p53 with MDM2—fine mapping of the MDM2 binding site on p53 using synthetic peptides. *Oncogene 9*, 2523–2529.
33. Kussie, P. H., Gorina, S., Marechal, V., Elenbaas, B., Moreau, J., Levine, A. J., and Pavletich, N. P. (1996) Structure of the MDM2 oncoprotein bound to the p53 tumor suppressor transactivation domain. *Science 274*, 948–953.
34. Cory, S., and Adams, J. M. (2002) The Bcl2 family: regulators of the cellular life-or-death switch. *Nat. Rev. Cancer 2*, 647–656.
35. Petros, A. M., Nettesheim, D. G., Wang, Y., Olejniczak, E. T., Meadows, R. P., Mack, J., Swift, K., Matayoshi, E. D., Zhang, H., Thompson, C. B., and Fesik, S. W. (2000) Rationale for Bcl-xL/Bad peptide complex formation from structure, mutagenesis, and biophysical studies. *Protein Sci. 9*, 2528–2534.
36. Schon, O., Friedler, A., Bycroft, M., Freund, S. M., and Fersht, A. R. (2002) Molecular mechanism of the interaction between MDM2 and p53. *J. Mol. Biol. 323*, 491–501.
37. Sakaguchi, K., Saito, S., Higashimoto, Y., Roy, S., Anderson, C. W., and Appella, E. (2000) Damage-mediated phosphorylation of human p53 threonine 18 through a cascade mediated by a casein 1-like kinase. Effect on Mdm2 binding. *J. Biol. Chem. 275*, 9278–9283.
38. Lee, H., Mok, K. H., Muhandiram, R., Park, K. H., Suk, J. E., Kim, D. H., Chang, J., Sung, Y. C., Choi, K. Y., and Han, K. H. (2000) Local structural elements in the mostly unstructured transcriptional activation domain of human p53. *J. Biol. Chem. 275*, 29426–29432.
39. Gao, G., Prutzman, K. C., King, M. L., Scheswohl, D. M., DeRose, E. F., London, R. E., Schaller, M. D., and Campbell, S. L. (2004) NMR solution structure of the focal adhesion targeting domain of focal adhesion kinase in complex with a paxillin LD peptide: evidence for a two-site binding model. *J. Biol. Chem. 279*, 8441–8451.
40. Guenther, R. H., Sit, T. L., Gracz, H. S., Dolan, M. A., Townsend, H. L., Liu, G., Newman, W. H., Agris, P. F., and Lommel, S. A. (2004) Structural characterization of an intermolecular RNA-RNA interaction involved in the transcription regulation element of a bipartite plant virus. *Nucleic Acids Res. 32*, 2819–2828.
41. Moll, U. M., Wolff, S., Speidel, D., and Deppert, W. (2005) Transcription-independent pro-apoptotic functions of p53. *Curr. Opin. Cell Biol. 17*, 631–636.
42. Chipuk, J. E., and Green, D. R. (2003) p53's believe it or not: lessons on transcription-independent death. *J. Clin. Immunol. 23*, 355–361.
43. Sayan, B. S., Sayan, A. E., Knight, R. A., Melino, G., and Cohen, G. M. (2006) p53 is cleaved by caspases generating fragments localizing to mitochondria. *J. Biol. Chem. 281*, 13566–13573.
44. Sot, B., Freund, S. M., and Fersht, A. R. (2007) Comparative biophysical characterization of p53 with the pro-apoptotic BAK and the anti-apoptotic BCL-xL. *J. Biol. Chem. 282*, 29193–29200.